ISSN 2706-655X Vol.6, Issue 4: 75-82, DOI: 10.25236/IJFET.2024.060413

Numerical simulation of cylinder under different natural frequency ratios

Dexin Liu[1,a], Hongyuan Sun[1,b,*], Qiang Xu[2,c], Jin Miao[1,d]

[1]School of Naval Architecture and Port Engineering, Shandong Jiaotong University, Weihai, Shandong Province, 264209, China
[2]Yantai CIMC Raffles Ocean Engineering Co., Ltd., Yantai, 264670, China
[a]liu516016362@163.com, [b]hongyuan_000@163.com, [c]53115703@qq.com, [d]15589425509@163.com
[*]Corresponding author

Abstract: *This paper adopts the computational fluid dynamics (CFD) method, firstly compares with the classic experiment of Jauvtis and Williamson in 2004, and verifies the reliability of numerical simulation. Then the vortex-induced motion response of cylindrical structures with different ratios of natural frequencies of the in-line to the transverse natural frequency ratio (natural frequency ratio, $f^*=f_{nx}/f_{ny}$) is numerically simulated. Through research, it is found that the natural frequency ratio is an important parameter affecting the vortex-induced motion characteristics of cylindrical structures. With the increase of the natural frequency ratio f^*, the response amplitude gradually increases and the cross-flow amplitude peak appears at a higher reduced speed, and the force-displacement curve undergoes a "phase switching" phenomenon; the change of the natural frequency ratio has little effect on the "locking" range of vortex-induced motion; at a specific reduced speed, the change of the natural frequency ratio will affect the vortex shedding mode, and the different vortex shedding modes that appear cause its motion trajectory to present an "8" shape with different tilt directions.*

Keywords: *Vortex-induced vibration; natural frequency ratio; two-degree-of-freedom; fluid-structure interaction; trajectories*

1. Introduction

At specific speed ranges, when ocean currents flow past bluff bodies, vortices are generated behind them, resulting in periodic in-line pulsating drag and transverse pulsating lift. This phenomenon, known as vortex-induced vibrations (VIV), is widely observed in practical engineering applications. For instance, VIV occurs in foundational cylindrical structures commonly found in marine risers and Spar platforms under certain wind speeds or ocean currents. Prolonged periodic vibrations can lead to structural damage and shorten the service life of these structures. Therefore, it is imperative to conduct further in-depth research on vortex-induced vibrations. The VIV response is influenced by numerous parameters, including reduced velocity, Reynolds number, mass ratio, stiffness, natural frequency ratio, and damping ratio.

Early studies on VIV primarily focused on the single degree of freedom (1DOF) of a cylinder, allowing only transverse vibration. Sarpkaya[1], Williamson and Govardhan[2] conducted relevant reviews on this topic. Feng[3] conducted experiments on vortex-induced vibrations of cylinders in air and found that the vibration amplitude curve exhibited two distinct branches. With the continuous development of ocean engineering, more experiments have been conducted underwater. Khalak and Williamson[4] observed that when the mass ratio of elastically supported cylinders is between 5 and 10, a higher amplitude upper branch appears. They also found that for larger mass ratios, the ratio of the transverse vibration frequency in the lock-in region to the natural frequency of the structure is approximately 1, while for smaller mass ratios, this ratio is less than 1. Govardhan and Williamson[5] proposed that there is a critical mass ratio. When the mass ratio is below this critical value, the range of the lock-in region becomes infinite.

Based on research into transverse single degree of freedom vibration, researchers discovered that the in-line degree of freedom significantly influences the VIV response characteristics. Dahl[6] conducted two-degree-of-freedom (2DOF) experiments on an elastically mounted rigid cylinder, finding that the maximum transverse amplitude exceeded 1.35D (where D is the cylinder diameter), while the in-line response reached 0.6D.With the introduction and advancement of two-degree-of-freedom (2DOF)

ISSN 2706-655X Vol.6, Issue 4: 75-82, DOI: 10.25236/IJFET.2024.060413

vortex-induced vibrations, the impact of the natural frequency ratio on vibration response has naturally become a focus of research. Most VIV studies have concentrated on the natural frequency ratio (the ratio of the in-line to transverse natural frequencies, $f^*=f_{nx}/f_{ny}$) being equal to 1. However, recent in-depth research has shown that when the natural frequency ratio deviates from 1, significant changes occur in the amplitude, motion trajectory, and vortex shedding frequency of VIV. Dahl[7] analyzed the VIV response of cylinders under different natural frequency ratios and found that the phase relationship between in-line and transverse directions affects the cylinder's motion trajectory. Zhao [8] investigated the influence of different natural frequency ratios on the vortex shedding patterns of cylinders under low Reynolds number conditions. Kang and Jia [9] conducted a series of 2DOF VIV experiments on cylinders under various conditions, summarizing the changes in amplitude response for different in-line and transverse natural frequencies. They identified various motion trajectory shapes, such as "crescent," "egg," and "raindrop," in addition to the typical "figure-eight" shape.

This study employs computational fluid dynamics (CFD) numerical simulations combined with dynamic mesh technology to analyze the impact of varying natural frequency ratios on the VIV characteristics of cylinders. The analysis focuses on response amplitude, response frequency, motion trajectory, and vortex shedding patterns.

2. Numerical model

2.1 Governing Equations

In this study, the cylindrical structure is simplified into a mass-spring-damper system, as illustrated in figure 1.

The governing equations are as follows:

$$m\frac{d^2x}{dt^2}+C_x\frac{dx}{dt}+K_x x=F_D(t) \tag{1}$$

$$m\frac{d^2y}{dt^2}+C_y\frac{dy}{dt}+K_y y=F_L(t) \tag{2}$$

t—Time; m—Structural Mass; C_x—Damping Coefficient in the Longitudinal Direction; C_y—Damping Coefficient in the Transverse Direction; K_x—Stiffness of the System in the Longitudinal Direction; K_y—Stiffness of the System in the Transverse Direction; x—Displacement of vortex-induced vibrations in the Longitudinal Direction; y—Displacement of vortex-induced vibrations in the Transverse Direction; $F_D(t)$ —Net Force per Unit Length in the Longitudinal Direction; $F_L(t)$ —Net Force per Unit Length in the Transverse Direction on the Cylinder.

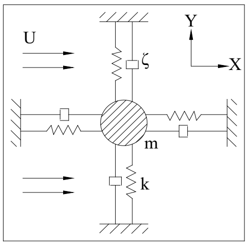

Figure 1: Underlying structure vortex induced motion model

2.2 Mesh Generation and Solution Method

2.2.1 Computational Domain and Mesh Generation

As shown in figure 2, the computational region and mesh are defined as follows: the cylinder has a diameter D=0.1m, and the computational domain size is 20D×40D.The cylinder's center is positioned at the coordinate origin. The velocity inlet is located 10D from the cylinder center, and the pressure outlet is 30D from the cylinder center. The top and bottom boundaries are 10D from the cylinder center. The cylinder surface boundary is set as a no-slip condition. The coupling between the base structure and the fluid is achieved using the overset mesh technique in Fluent. Overset meshes are used to discretize

ISSN 2706-655X Vol.6, Issue 4: 75-82, DOI: 10.25236/IJFET.2024.060413

computational domains with two or more overlapping meshes, offering advantages for handling moving body problems. In the Fluent 2D simulation, the SST k-ω turbulence model is chosen, which requires a high-quality mesh. The body-fitted mesh near the wall must be set within the viscous sublayer, and a finely structured mesh is necessary near the wall. The first layer height of the near-wall mesh must satisfy y+<1. Therefore, 10 layers of boundary layer mesh are set near the wall.

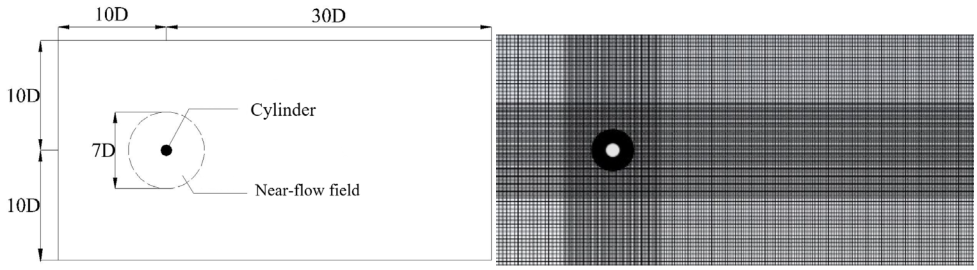

Figure 2: Computing regional and overall flow fields and displaying the mesh

2.2.2 Solution Method

The Fluent solver is utilized to simulate the surrounding flow field. During the solution process, a User Defined Function (UDF) is embedded into the Fluent solver, employing the Compute_Force_And_Moment function to extract fluid forces. Given that fluid forces can be considered constant within sufficiently small time-steps, the fourth-order Runge-Kutta method is directly used to discretize the motion equations, thereby determining the cylinder's velocity and displacement at each time step. The dynamic mesh technology is employed to update the flow field mesh in a timely manner. In the solution process, transient computation methods are used, with the SST k-ω model selected for turbulence modeling. The pressure-velocity coupling in the momentum equation is handled using the SIMPLEC algorithm, and second-order upwind schemes are applied to momentum, turbulence kinetic energy, and dissipation rate.

2.3 Validation of the numerical methods

2.3.1 Calculation Conditions

In order to ensure the rationality and reliability of the calculation results of vortex-induced motion by the calculation model and parameters, the classic experiment of Jauvtis and Williamson[10] in 2004 was selected as a control to verify the numerical simulation results, where the mass ratio m^*=2.6, the damping ratio ζ=0.0036, the natural frequencies in the downstream and cross-stream directions are equal f_{nx}=f_{ny}=0.4Hz (that is, the natural frequency ratio f^* is 1), and the reduced speed is 3~13. The specific working condition information is shown in Table 1. Then three groups of calculation models were selected, and different numbers of grids were considered to verify the grid independence. The results are shown in Table 2. Through comparison, this paper selected grid B as the optimal solution.

Table 1: Calculate the working condition data cables

Numble	m^*	ζ	f_{nx}/H_z	f_{ny}/H_z	f^*	$U_{C/m\cdot s\text{-}1}$	U_r
1	2	0.05	0.19	0.38	0.5	0.05~0.81	1.32~21.32
2	2	0.05	0.57	0.38	1.5	0.05~0.81	1.32~21.32
3	2	0.05	0.76	0.38	2	0.05~0.81	1.32~21.32
4	2.6	0.0036	0.40	0.40	1	0.09~0.67	2~13

Table 2: Mesh simulation results

Mesh	A	B	C
Number of units	20328	28694	34561
$A_{y\max}$	0.924	0.979	0.979
$A_{x\max}$	0.162	0.176	0.178
C_l	3.359	3.897	3.898
C_d	2.045	2.352	2.354

2.3.2 Amplitude Comparison

Figure 3 shows the comparison between the dimensionless amplitudes obtained from numerical simulations and experimental results at different reduced velocities. According to the theory of vortex-

ISSN 2706-655X Vol.6, Issue 4: 75-82, DOI: 10.25236/IJFET.2024.060413

induced motion, the response can be divided into three branches: the initial branch, the upper branch, and the lower branch. From figure 3, it is evident that the trend of the dimensionless amplitude curves from numerical simulations matches closely with the experimental results, indicating a high degree of agreement. However, at U_r=7, the numerical simulation does not reach the maximum transverse amplitude observed in the experiments, and the longitudinal amplitude is similarly underestimated at its peak value. The primary reasons for these discrepancies are as follows:(1) There are certain errors in the processing of experimental apparatus components or slight deviations in assembly, resulting in greater friction during the motion. This causes the overall numerical simulation results to deviate somewhat from the experimental results. (2) the upper branch, the cylinder's motion amplitude is relatively large, significantly reducing the axial correlation of the cylinder. However, in the 2D numerical simulations of the cylinder, it is assumed that the axial correlation is complete.

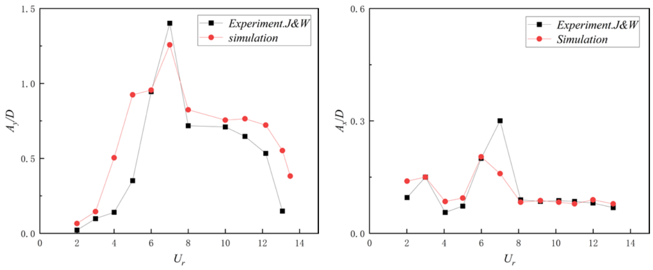

Figure 3: Results verification of vortex motion results

3. Results and discussion

3.1 Cylinder Response Amplitude

Figure 4presents the amplitude variation curves of the cylinder with different natural frequency ratios as a function of reduced velocity. As shown in figure 4, the transverse amplitude curve initially increases and then decreases with increasing reduced velocity. Moreover, with the increase in natural frequency ratio, the reduced velocity corresponding to the maximum amplitude also increases.t is evident that the in-line amplitude curve exhibits a similar trend, initially increasing and then decreasing with increasing reduced velocity. During the initial branch phase, the in-line amplitude curve is relatively sensitive to changes in the natural frequency ratio, showing significant differences in amplitude peaks. For natural frequency ratios f^* of 0.5 and 1.5, the in-line amplitude peaks occur around U_r =5. When the natural frequency ratio is 2, the in-line amplitude peak occurs around U_r =7.

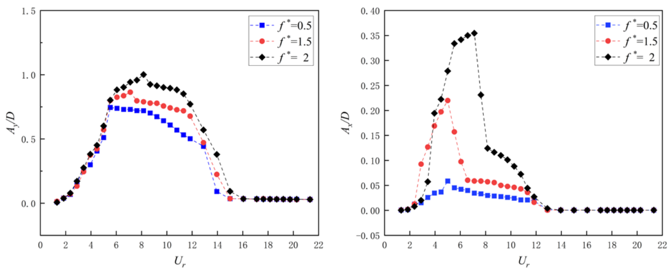

Figure 4: Variation of transverse flow amplitude with reduced velocity at different natural frequency ratios

3.2 Cylinder Frequency Response

To clearly and intuitively observe the "lock-in" region of vortex-induced motion (VIM), the in-line vibration frequency f_x and transverse vibration frequency fy are normalized by the transverse natural frequency f_{ny}. Figure 5 presents the variation curves of VIV response frequencies with reduced velocity for the cylinder under different natural frequency ratios. As illustrated in Figure 5, the "lock-in" region for both the in-line vibration frequency f_x and the transverse vibration frequency f_y occurs within U_r =7.11 to 15, where f_x/f_{ny} and f_y/f_{ny} remain almost constant. Beyond the "lock-in" region, both f_y/f_{ny} and f_x/f_{ny} increase sharply, followed by a linear increase in growth rate. The transverse vibration frequency approaches the Strouhal frequency, while the in-line vibration frequency is twice the Strouhal frequency. Consequently, the ratio of the in-line vibration frequency f_x to the transverse vibration frequency f_y

ISSN 2706-655X Vol.6, Issue 4: 75-82, DOI: 10.25236/IJFET.2024.060413

consistently approaches 2:1.

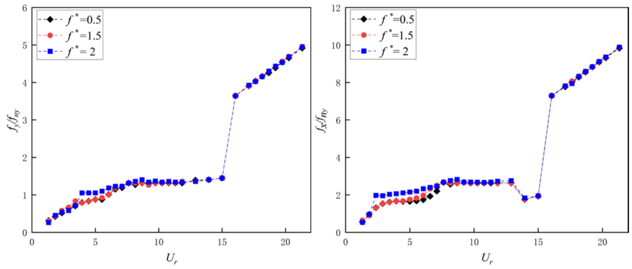

Figure 5: Diagram of the response frequency varies with the reduction velocity at different natural frequency ratios

3.3 Time history curve of transverse displacement and lift coefficient

The time history curve describes the displacement and lift changes of the Spar type floating foundation structure over time, and can directly observe the change process of the transverse displacement over time. Figures 6, 7, and 8 list the time history curves of the vortex-induced motion lift Cl and the transverse displacement of three natural frequency ratios respectively. Due to the large number of working conditions, this paper mainly selects the time history curves of different natural frequency ratios under the three conditions of reduced speed U_r =3.95, U_r =5, and U_r =11.84 for analysis.

Figure 6 When the reduced speed U_r =3.95, the time history curves of displacement and force of f^*=0.5 show obvious periodicity, the peak positions of the y/D time history curve and the Cl time history curve are the same, the phase angles are basically equal, and the lift and displacement are synchronized, indicating that the transverse motion is caused by lift, and the *y/D* curve and C_l curve of f^*=1.5 and 2 show "beating" phenomenon. As the reduced speed increases, in Figure 7, when the reduced speed U_r =5, the "phase switching" phenomenon occurs. Under the conditions of the natural frequency ratio f^*=0.5 and 1.5, the phases of the *y/D* and C_l curves are in phase. As the natural frequency ratio increases, the phases of the two curves become out of phase when the natural frequency ratio f^*=2. Figure 8 When the reduced speed U_r =11.84, regardless of the VIM under any natural frequency ratio condition, the lift and displacement are completely out of sync, with a phase difference of about 180 degrees, and as the natural frequency ratio f* increases, the mean value of the lift coefficient increases.

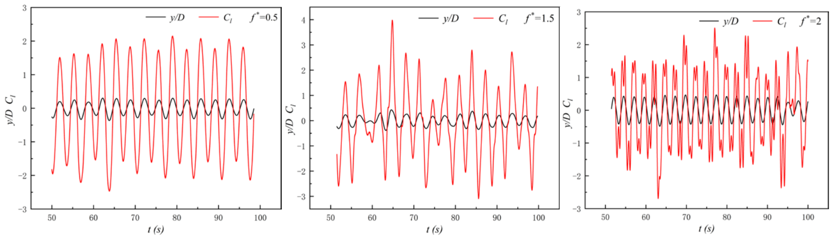

Figure 6: Time history curves of C_l and y/D under U_r =3.95

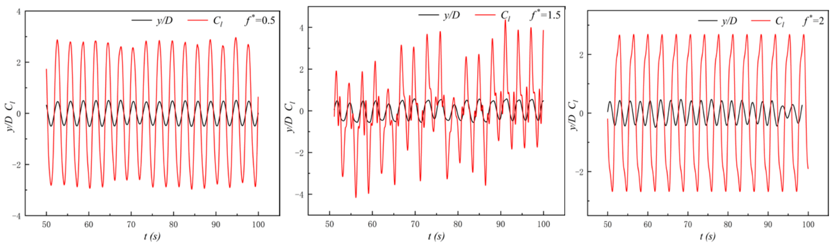

Figure 7: Time history curves of C_l and y/D under U_r =5

ISSN 2706-655X Vol.6, Issue 4: 75-82, DOI: 10.25236/IJFET.2024.060413

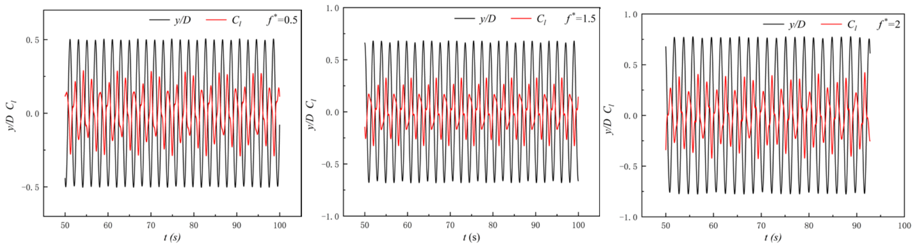

Figure 8: Time history curves of C_l and y/D under U_r =11.84

3.4 Trajectories

As shown in Figure 9, with the increase of the natural frequency ratio, the vortex-induced motion response amplitude increases, and the motion trajectory presents more forms from simple to complex. Most of the motion trajectories show an "8" shape. When the reduced speed is small, the amplitude of the downstream motion is small, and the cross-stream motion dominates. With the increase of the reduced speed, the motion trajectories under different natural frequency ratios gradually converge, showing an elongated "8" shape. When the natural frequency ratio f^*= 0.5, the amplitude is small in the initial branching stage, and the motion trajectory is not obvious. With the increase of the reduced speed, the motion trajectory gradually presents an "8" shape and is relatively slender. This is because the amplitude in the downstream direction is smaller than that in the cross-flow direction and the main peak frequency of the downstream motion is the same as the cross-flow motion frequency; when the natural frequency ratio f^*= 1.5, the initial branch presents a "crescent" shape. With the increase of the reduced speed, the motion trajectory gradually changes to an inclined "8" shape. This inclined "8" shape motion trajectory may cause asymmetry in vortex discharge; when the natural frequency ratio f^*= 2, with the increase of the reduced speed, the motion trajectory changes from an "inverted C" shape to a regular "8" shape.

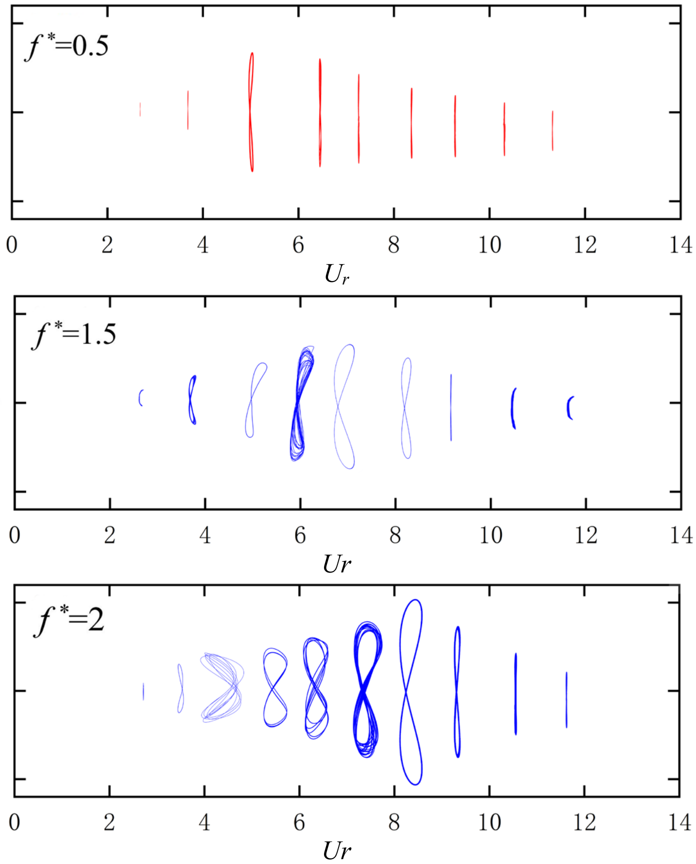

Figure 9: Variation of the orbital trajectories with the reduced velocity at different natural frequency ratios

By observing the relationship between the direction of motion trajectory and the direction of fluid flow, we can understand the extent of VIV's impact on the structure and the interaction mechanism

ISSN 2706-655X Vol.6, Issue 4: 75-82, DOI: 10.25236/IJFET.2024.060413

between structural response and fluid flow. A sudden change in the direction of the motion trajectory may indicate that the structure is in an unstable state. Previous research has shown that when the natural frequency ratio is 2, the amplitude is relatively large, posing significant risks to the engineering structure. Therefore, analyzing the motion trajectory direction helps prevent structural fatigue damage. Figure 10 presents the motion trajectory directions at different reduced velocities for a natural frequency ratio of 2, with the direction of motion indicated by arrows. As seen in Figure 10, at U_r =4.47, the in-line flow direction is the same as the incoming flow direction, and the motion trajectory is clockwise. At U_r =6.05, under the combined influence of transverse and in-line drag, the motion follows a classic figure-eight trajectory, with the in-line direction moving from right to left, opposite to the incoming flow direction, resulting in a counterclockwise motion trajectory. For U_r >6.05, the motion trajectory continues to maintain a counterclockwise direction and becomes dominant.

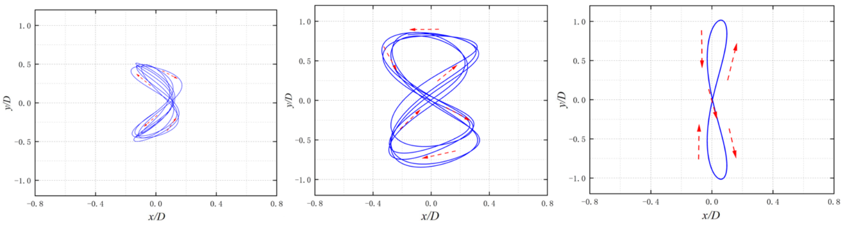

Ur=4.47 *Ur=6.05* *Ur=8.16*

Figure 10: Variation in the direction of motion trajectory under different reduction velocities

3.5 Vortex pattern in wake

Based on the generation and evolution of vortex structures, vortex shedding modes can be classified into four distinct types: 2S, 2T, 2P, and P+S. Figure 11shows the instantaneous vorticity diagram of the cylinder at typical reduced speeds under different natural frequency ratios. As shown in Figure 11(a), when the natural frequency ratio is 0.5, at U_r =3.95 in the "initial branch," the vortex shedding mode is 2S, which means a pair of single vortices is shed per cycle. With the increase in reduced velocity, at U_r =5, the vortex shedding mode changes to 2T, where three vortices are shed per cycle, corresponding to the "upper branch." At U_r =11.84, in the "lower branch," the vortex shedding mode transitions to 2P, where two pairs of vortices are shed per cycle. As illustrated in Figure 11(b), when the natural frequency ratio is 1.5, at U_r =3.95, the vortex shedding mode is the same as that for 0.5, which is 2S. As the reduced velocity increases, at U_r =5, the vortex shedding mode changes to P+S, where one vortex and one pair of vortices are shed per cycle. This asymmetric vortex shedding mode may cause the motion trajectory to exhibit a skewed figure-eight shape. At U_r =11.84, the vortex shedding mode changes to 2P.

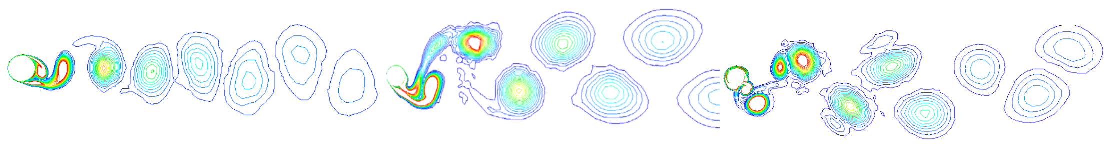

Ur=3.95 *Ur=5* *Ur=11.84*

(a) The vortex distribution of f^*=0.5 at different reduced velocities

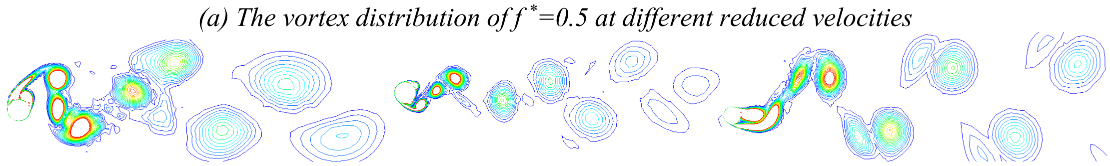

Ur=3.95 *Ur=5* *Ur=11.84*

(b) The vortex distribution of f^*=1.5 at different reduced velocities

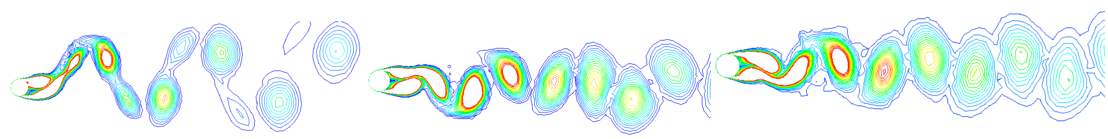

Ur=3.95 *Ur=5* *Ur=11.84*

(c) The vortex distribution of f^*=2 at different reduced velocities

Figure 11: Vorticity contours of different reduced velocities and natural frequency ratio

ISSN 2706-655X Vol.6, Issue 4: 75-82, DOI: 10.25236/IJFET.2024.060413

4. Summary

By combining CFD numerical simulation method with dynamic mesh technology, numerical simulation of cylinders with natural frequency ratios of 0.5, 1.5, and 2 was carried out, mainly analyzing the response amplitude, response frequency, motion trajectory, and vortex shedding mode of the cylinder VIV. The following conclusions were drawn:

(1) The reliability of numerical simulation was verified by comparing with the classic experiment of Jauvtis and Williamson in 2004.

(2) The larger the natural frequency ratio, the larger the maximum amplitude of vortex-induced motion; the maximum amplitude in the transverse direction shifts to a larger reduced velocity as the natural frequency ratio increases. The locking ranges of the three non-natural frequency ratios are the same, and the ratio of the vibration frequency in the downstream and transverse directions is always close to 2:1 in a wider reduced velocity range. Most of the motion trajectories under different natural frequency ratios present different shapes of "8". When the natural frequency ratio is 2, as the reduced speed increases, the clockwise motion trajectory gradually decreases, and the counterclockwise motion trajectory gradually becomes dominant.

(3) At a specific reduced speed, the natural frequency ratio has a greater influence on the vortex leakage mode. When U_r=5, when the natural frequency ratio increases from 0.5 to 2, the force-displacement curve undergoes a "phase switching" phenomenon, and the corresponding vortex leakage mode changes from 2T mode to P+S mode and then to 2P mode. The asymmetric P+S mode may cause the motion trajectory to present an inclined "8" shape.

References

[1] Sarpkaya T. A critical review of the intrinsic nature of vortex-induced vibrations[J]. Journal of fluids and structures, 2004, 19(4): 389-447.
[2] Williamson C H K, Govardhan R. A brief review of recent results in vortex-induced vibrations[J]. Journal of Wind engineering and industrial Aerodynamics, 2008, 96(6-7): 713-735.
[3] Feng C C. The measurement of vortex induced effects in flow past stationary and oscillating circular and D-section cylinders[D]. University of British Columbia, 1968.
[4] Khalak A, Williamson C H K. Motions, forces and mode transitions in vortex-induced vibrations at low mass-damping[J]. Journal of fluids and Structures, 1999, 13(7-8): 813-851.
[5] Govardhan R, Williamson C H K. Modes of vortex formation and frequency response of a freely vibrating cylinder[J]. Journal of Fluid Mechanics, 2000, 420: 85-130.
[6] Dahl J M, Hover F S, Triantafyllou M S. Two-degree-of-freedom vortex-induced vibrations using a force assisted apparatus[J]. Journal of Fluids and Structures, 2006, 22(6-7): 807-818.
[7] Dahl J M, Hover F S, Triantafyllou M S, et al. Dual resonance in vortex-induced vibrations at subcritical and supercritical Reynolds numbers[J]. Journal of Fluid Mechanics, 2010, 643: 395-424.
[8] Zhao M. Effects of natural frequency ratio on vortex-induced vibration of a circular cylinder in steady flow[J]. Physics of Fluids, 2020, 32(7).
[9] KANG Z, JIA L S.An experiment study of a cylinder's two degree of freedom VIV trajectories[J]. Ocean Engineering, 2013, 70:129-140.
[10] Jauvtis N, Williamson C H K. The effect of two degrees of freedom on vortex-induced vibration at low mass and damping[J]. Journal of Fluid Mechanics, 2004, 509: 23-62.